Materials Science and Engineering B 280 (2022) 115711

Contents lists available at ScienceDirect

Materials Science & Engineering B

journal homepage: www.elsevier.com/locate/mseb

Effect of substrate-induced lattice strain on the electrochemical properties of pulsed laser deposited nickel oxide thin film

Jacob Som [a], Jonghyun Choi [b], Honglin Zhang [a], Nikhil Reddy Mucha [a], Svitlana Fialkova [a], Kwadwo Mensah-Darkwa [c], Jin Suntivich [d], Ram K. Gupta [b], Dhananjay Kumar [a,*]

[a] Department of Mechanical Engineering, North Carolina Agricultural and Technical State University, Greensboro, NC 27401, USA
[b] Department of Chemistry, Pittsburg State University, Kansas, KS 66762, USA
[c] Department of Materials Engineering, Kwame Nkrumah University of Science and Technology, Kumasi, Ghana
[d] Department of Materials Science and Engineering, Cornell University, Ithaca, NY 14853, USA

ARTICLE INFO

Keywords:
NiO thin film
Pulsed laser deposition
Lattice strain
Hydrogen evolution reaction
Cyclic voltammetry

ABSTRACT

The storage of renewable energy is an important step toward the global effort to combat air contamination and climate change. In this work, the influence of substrate-induced strain on the electrocatalytic properties of nickel oxide (NiO) films toward the hydrogen evolution reaction (HER) is studied. Using pulsed laser deposition, NiO thin films were deposited on strontium titanate, lanthanum aluminate, and sapphire substrates to examine how the substrate–film lattice mismatch influences the electrochemical properties. It was observed that the electrocatalytic activities of the NiO thin films exhibited strong sensitivity to strain; the NiO film with the smallest strain recorded the lowest overpotential for the HER. The NiO films were further explored to estimate the charge storage capacity and surface roughness. This work shows the use of simple thin-film synthesis as a way to evaluate the strain effect in electrocatalysis.

1. Introduction

The exponential population growth coupled with high-standard living demands have resulted in today's unprecedented energy and environmental crisis. Over the next two decades, the energy demand is projected to increase by 50%, with the average global power requirement anticipated to reach 30–46 TW by 2100 [1,2]. In addition to the growing energy demand, there are concerns regarding natural resources' depletion as well as the associated environmental and socio-economic impacts stemming from the combustion and over-exploitation of petrochemicals [3–6]. Thus, sustainable energy is one of the most important priorities in the 21st century. Hydrogen is a promising clean energy option due to its zero-emission nature, storage convenience, versatility, and high energy density [7–10]. Hydrogen can be produced by electrical power through electrolysis, where water is split into hydrogen and oxygen fuels [11]. Fuel cells, on the other hand, reverse the process to generate energy [9]. Electrocatalysts are integral in the water-splitting processes as they increase the rates of the two electrochemical reactions during water splitting: the hydrogen evolution reaction (HER) and oxygen evolution reaction (OER) [12,13]. Transition metals such as nickel (Ni), titanium (Ti), iron (Fe), cobalt (Co), copper (Cu), and their mixtures have been widely studied for these applications due to their abundance and, hence, cost efficiency as compared to the conventionally used precious metals such as platinum (Pt), palladium (Pd), ruthenium (Ru), and iridium (Ir) [1,14–16]. Ni compounds have received substantial attention as an electrocatalyst for HER, OER, and oxygen reduction reaction (ORR) [17], having demonstrated low overpotential, high corrosion resistance, low cost, and abundance [6,18,19]. NiO is one of the few known p-type oxides with excellent electrochemical capabilities [20–22]. It is, therefore, a great platform for the fundamental electrochemical studies of p-type oxides. P-type oxides can serve as a photoelectrode in a solar-driven water-splitting cell, when integrating with n-type materials such as titanium oxynitrides [14,23]. Our choice to investigate NiO is driven by this view that NiO holds a great future for photoelectrochemistry. It is important to point out that our findings can likely be extended to other Ni-based materials. Many groups have shown that the surface layers of NiP and NiS can transform to Ni-oxide species during electrochemistry [24,25]. We, therefore, believe that our results help elucidate how Ni-based compounds can be used for capacitors, batteries, sensors, catalysis and as a protective layer

* Corresponding author.
E-mail address: dkumar@ncat.edu (D. Kumar).

https://doi.org/10.1016/j.mseb.2022.115711
Received 27 September 2021; Received in revised form 27 February 2022; Accepted 22 March 2022
Available online 25 March 2022

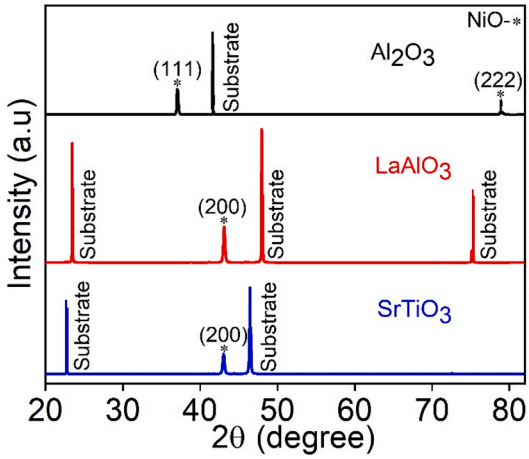

Fig. 1. X-ray diffraction patterns of the NiO thin films grown on different substrates.

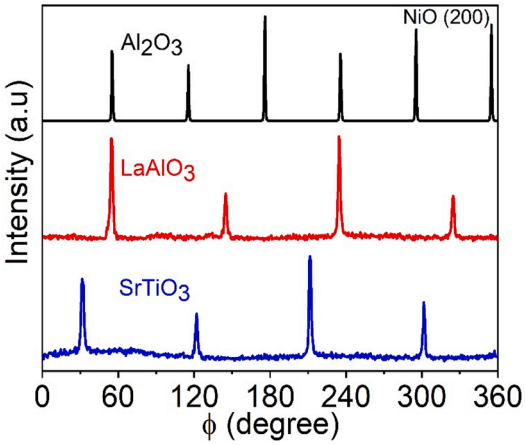

Fig. 2. Phi Scan of NiO (2 0 0) plane on $SrTiO_3$, $LaAlO_3$ and Al_2O_3 substrates.

for the anodic part of a p-n buried junctions in integrated water-splitting systems [26,27]. There are different NiO-thin film synthesis routes including spin coating [28], thermal evaporation [29], D.C. reactive magnetron sputtering [30], spray pyrolysis [31], R.F. sputtering [32] and pulsed laser deposition (PLD) [33]. These methods use different optimization parameters, which lead to a variation in the thin film properties. Among these, the ability to produce uniform thin films with well-controlled thickness and surface structure makes PLD an attractive deposition process [34–37]. In this study, we investigate the substrate-dependent electrochemical properties of PLD-prepared NiO thin films. To explore this, we have fabricated NiO thin films on strontium titanate ($SrTiO_3$), lanthanum aluminate ($LaAlO_3$), and Sapphire (Al_2O_3) substrates.

2. Materials and methods

NiO thin film samples were synthesized on (0 0 0 1) single-crystal sapphire, (1 0 0) strontium titanate, and (1 0 0) lanthanum aluminate substrate using PLD. High-purity NiO target was used to deposit the NiO films. A KrF laser (Coherent Complex Pro, wavelength 248 nm, pulse duration 30 ns, repetition rate 10 Hz) was used. A fixed number of laser pulses (shots) of 10,000 (deposition time = 2000 s) was used. We set the substrate temperature at 400 °C and oxygen pressure at 60 mTorr using the laser energy density at 2 J/cm^2. The crystallographic orientation and phase purity of the NiO films were studied using X-ray diffraction (XRD, Bruker D8). The surface topography was characterized using an atomic force microscope (NTEGRA Prima) at ambient conditions (in air, 22 °C, and relative humidity below 40 %) using the contact mode with the resolution of 10 nm per point. A scan speed of 9 μm/s or lower was used for all measurements. The electrical resistivity was determined using a standard four-probe measurement.

The electrochemical activities of NiO samples were analyzed using linear sweep voltammetry (LSV), cyclic voltammetry (CV), and electrochemical impedance spectroscopy (EIS). The electrochemical properties were studied using an electrochemical workstation (Versatat 4–500, Princeton Applied Research, USA). A three-electrode system was used for all these measurements: a reference electrode (Hg/HgO), a counter electrode (platinum), and a working electrode (NiO thin films). The electrolyte solution used was 1 M KOH. LSV and EIS measurements were performed at a rate of 5 mV/s and 0 V, respectively. The geometric area of the sample submerged in the electrolyte was 24 mm^2, which was used in the calculation of current density. From the commercial standpoint, this surface area is not sufficient for water electrolysis, which requires significantly larger areas (>100 cm^2). It should be noted that the objective of this research is to understand the fundamental structure–property relationship of NiO thin films, not to scale up NiO films for commercial applications. To meet the commercialization target, the results from the PLD technique will have to be translated to more cost-effective deposition techniques such as sputtering, spin coating, or electrophoretic deposition. However, such efforts are beyond the scope of the present work. All the electrochemical data were analyzed after iR correction, using the solution resistance obtained from the EIS measurement at 0 V vs. Hg/HgO.

3. Results and discussion

3.1. Morphological and topographical characteristics

XRD peaks were indexed for the NiO thin films grown on different substrates under identical growth conditions, using the 2θ scan from 20° to 80° angle. The results are plotted in Fig. 1, which shows a peak at 2θ = 43° corresponding to the (2 0 0) orientation of the NiO film on $SrTiO_3$ and $LaAlO_3$ substrates. Interestingly, the NiO film grown on the Al_2O_3 substrate favored the growth in different orientation. These XRD peaks are attributed to (1 1 1) and (2 2 2) NiO at 2θ = 37° and 78°, respectively. The appearance of narrow peaks with particular orientation suggests that the films are highly textured. The epitaxial nature of the NiO films on all three substrates was confirmed by the phi (ϕ)-scan of Ni (2 0 0) peak as presented in Fig. 2. In the case of the NiO films grown on $SrTiO_3$ and $LaAlO_3$ substrates, there are four peaks spaced at 90° [38–40]. In the case of the hexagonal sapphire substrate, the NiO film acquires a hexagonal structure as reflected by the appearance of the six peaks spaced at 60° in the ϕ - scan. It can be seen that the preferential orientation and crystallinity of the NiO film depend on the substrate type. Given that the surface orientation of the thin film electrocatalyst have different planar densities and different interatomic distance, we expect them to affect their interactions with the electrolyte. In the following, we will discuss

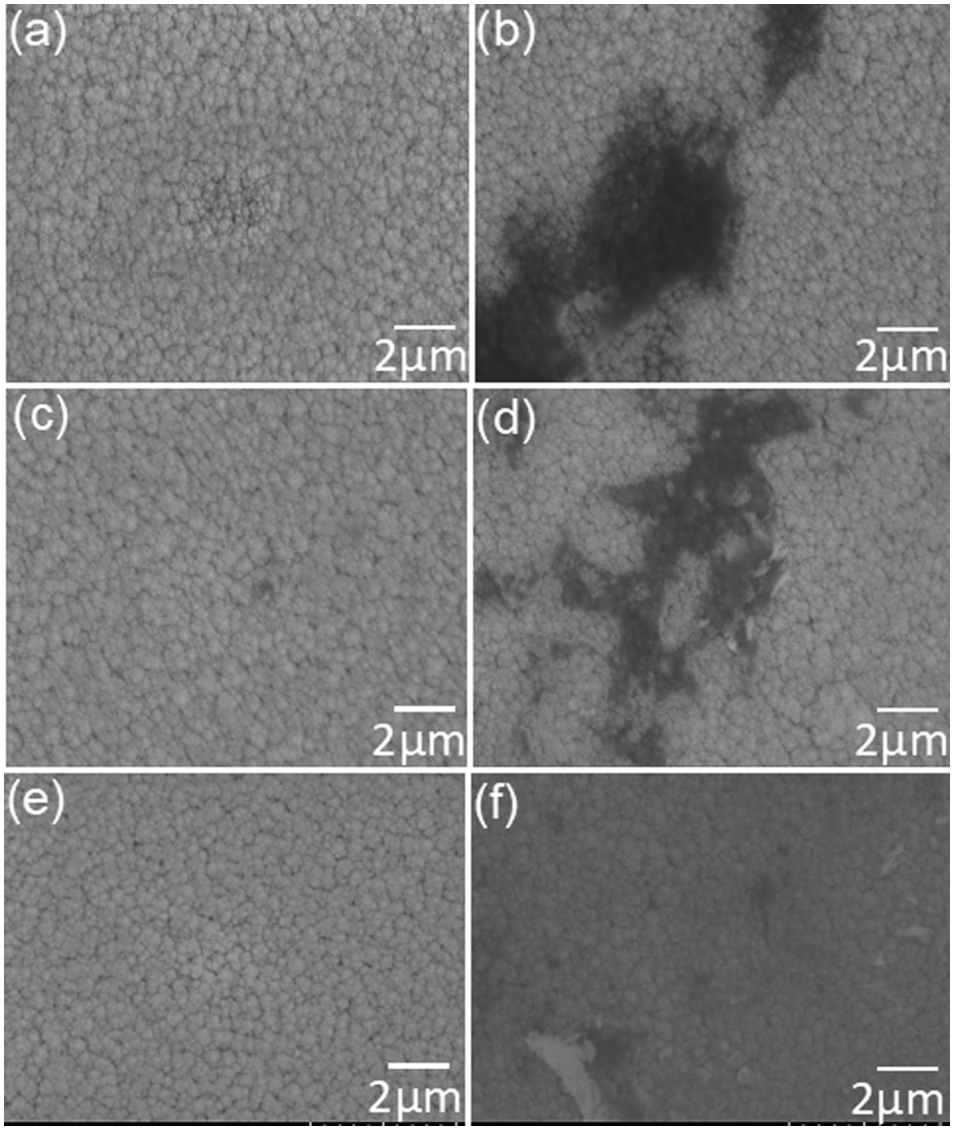

Fig. 3. FE-SEM images at the magnification of 20,000 of the NiO films grown on $SrTiO_3$ (a) before and (b) after electrolysis; $LaAlO_3$ (c) before and (d) after electrolysis; Al_2O_3 (e) before and (f) after electrolysis.

the relationship between NiO films with different orientations and different strain levels and their electrochemical properties.

The surface morphology of NiO films was analyzed by recording SEM images before and after each electrochemical test to understand behaviors of the NiO thin films in the electrochemical solutions under applied currents. The images in Fig. 3 on the left (a, c, and e) represent the surface morphology before, and the images on the right (b, d, and f) in the same row are the surface morphology of the same sample after. We observe the formation of fine pits. Thermodynamically, the reduction of NiO to Ni is expected to occur near the HER.

The formation of these pits could occur as a result of this reduction during Ni redox cycling [41]. The topographical images of the NiO thin films (Fig. 4a-c) were recorded using AFM. The surface roughness of the NiO thin films on $SrTiO_3$, $LaAlO_3$, and Al_2O_3 has been found to be 9.69, 3.63, and 1.58 nm, respectively. Rougher film texture on the nanoscale results in a larger electrode/electrolyte interfacial area. These surface roughness values are consistent with the charge-storage trend on the NiO films.

The surface electronic and oxidation state of the NiO thin films grown on Al_2O_3, $LaAlO_3$, and $SrTiO_3$ were assessed via XPS analysis. The thickness of these films, measured with a surface profilometer, was found to be 240 ± 5 nm on all three substrates. The thickness value is in agreement with the thickness value inferred from the etch rate and time taken to reach the substrate surface while recording the depth profile in XPS. The XPS spectra were calibrated with the C 1s peak to 284.6 eV. The survey scan (Fig. 5a) certifies the presence of Ni, O, and C without

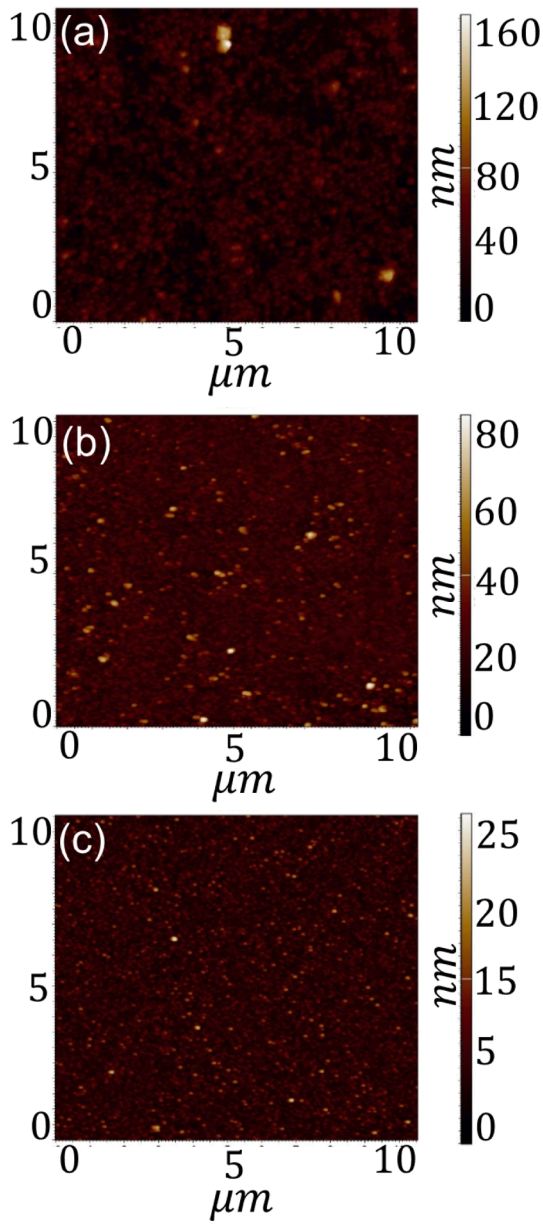

Fig. 4. AFM topography profiles of NiO films grown on (a) $SrTiO_3$, (b) $LaAlO_3$ and (C) Al_2O_3 substrates.

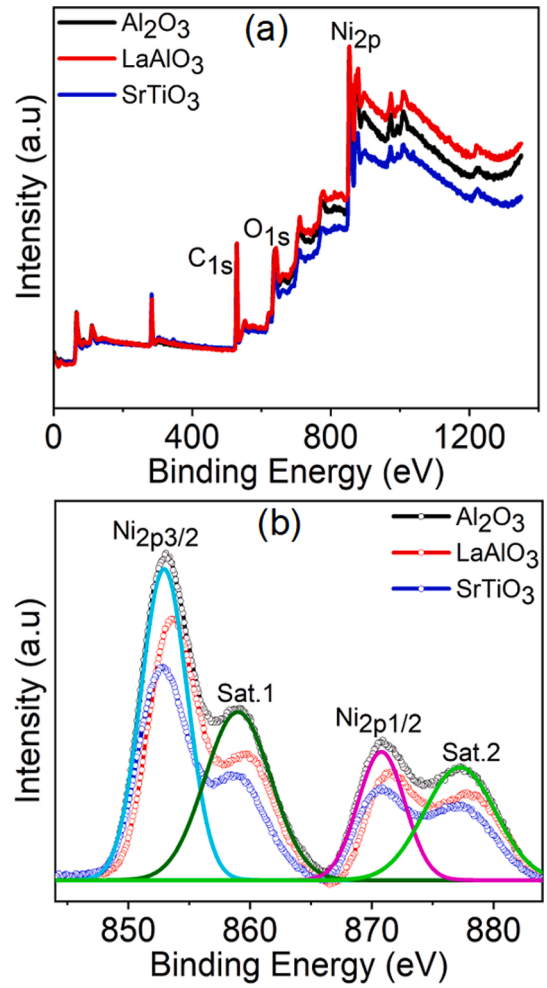

Fig. 5. XPS spectra of (a) Survey Scan (b) Ni 2p peaks.

any other elements in the films. This is consistent with the XRD micrographs obtained in Fig. 1, showing only peaks for the NiO films and the respective substrates. The presence of C is attributed to the atmospheric carbon [10]. The deconvoluted XPS spectrum of Ni_{2p} is shown in Fig. 5b, where the peaks located in the region 853–860 eV are marked as a satellite and a main peak corresponding to $Ni_{2p3/2}$. Shown also in this figure is the deconvoluted XPS spectrum of Ni_{2p} in 872–878 eV region with one satellite peak and one main peak that corresponds to $Ni_{2p1/2}$ [42,43]. The O 1s peak (Fig. 6) recorded from the NiO film on all the three substrates is centered at the binding energy of 528 eV which is attributed to the Ni-O metal–oxygen bond corresponding to the lattice O^{2-} ions in NiO [8,44]. The absence of additional peaks in the O 1s spectra suggests minimal surface oxygen and hydroxyl defects in our samples [37].

3.1.1. Lattice strain measurements

The full width half maxima (FWHM) of the (200) peak, grain size, and surface roughness are listed in Table 1. The percentage out-of-plane lattice strain and dislocation density are also presented in Table 1. The NiO interfacial substrate-film lattice strain, called the external strain (ε_{ext}) arising from the lattice mismatch between the NiO films and substrates is calculated using $\varepsilon_{ext} = (a_s - a_f)/a_f$, where a_s and a_f are the substrate and film lattice parameters, respectively. When a_s is smaller than a_f there is a compressive lattice strain in the film at the interfacial region, while a tensile strain is experienced in the interfacial region when the opposite is true. The percent lattice strain (ε) obtained for the films deposited on the $SrTiO_3$, $LaAlO_3$ and Al_2O_3, have been found as 7%, 10% and 12%, respectively. The NiO/ Al_2O_3 sample accounted for the highest strain of 12 % among the 3 samples. The dislocation density is calculated by taking inverse of D^2, where D is the average grain size of the NiO film determined using the Scherrer Equation [45], $D = K\lambda/\beta$

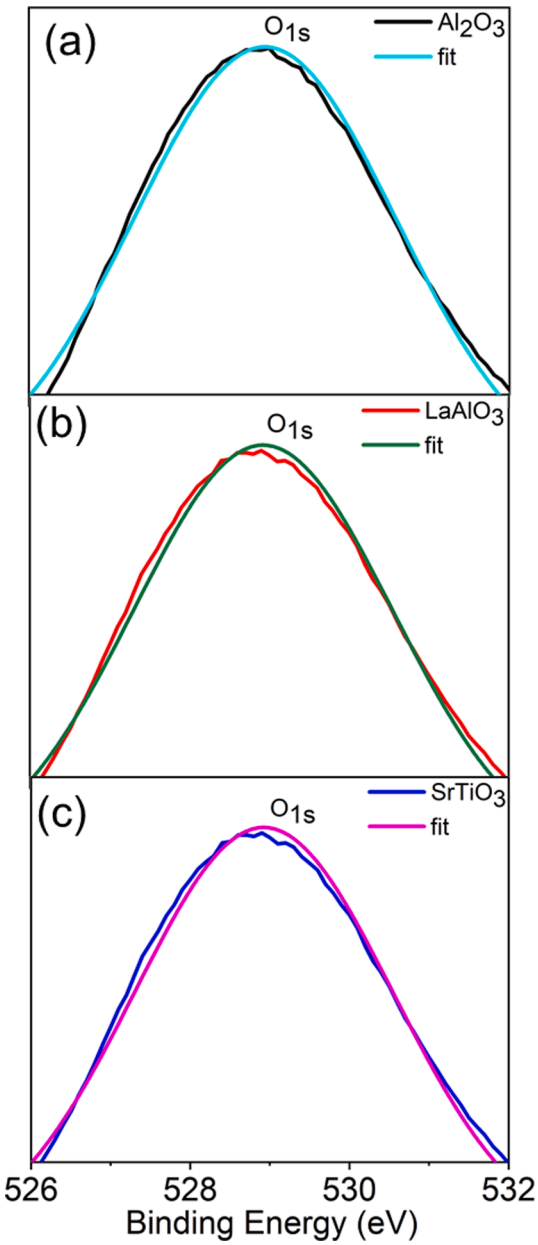

Fig. 6. O 1s XPS spectra recorded from sputtered clean NiO films deposited on (a) Al_2O_3, (b) $LaAlO_3$, and (c) $SrTiO_3$ substrates.

cosθ. Here K is the dimensionless shape factor close to unity, λ is the X-ray wavelength (=1.54 Å), β is FWHM, and θ is the Bragg angle. The presence of the dislocations in the NiO films impede the conduction of electrons leading to higher electrical resistivity as reflected from their four probe resistivity values of 5.7, 7.2, and 8.1 Ω-m for NiO/$SrTiO_3$, NiO/$LaAlO_3$ and NiO/Al_2O_3, respectively. The electrical resistivity was measured using the Van der Pauw method. Increasing electrical resistivity values in the NiO films are in accordance with the increase in the dislocation density measured in these films, i.e., 0.9, 1.1, and 1.9 ($\times 10^{15}$) m^{-2}, respectively [46,47].

3.2. Electrochemical properties

The electrochemical properties of the NiO films were investigated using linear sweep voltammetry (LSV) in 1 M KOH solution. The polarization curves of the NiO films are shown in Fig. 7a, where the current density (j) is plotted as a function of sweeping potential for three NiO thin film samples. As marked in this figure, the HER overpotential the NiO thin films on Al_2O_3, $LaAlO_3$, and $SrTiO_3$ substrates are 215 mV, 192 mV, and 120 mV, respectively. The reference potential was converted to RHE using the equation by considering the Hg/HgO standard potential (0.098 V vs. standard hydrogen electrode) and pH shift. We have used the 10 mA/cm^2 current density criterion as it is a metric for the overpotential requirement of a photoelectrochemical device [14,48]. The lowest overpotential for the HER electrocatalysis is observed on NiO/$SrTiO_3$. This observation is consistent with the presence of the high surface roughness of the NiO/$SrTiO_3$ sample, providing more active sites for electrocatalysis. The NiO/$SrTiO_3$ sample, as previously established, also displayed the lowest electrical resistivity. Therefore, the catalytic enhancement could also come from improved electron transferability, which has been reported for the oxygen electrocatalysis on $LaMnO_3$ [49].

The HER kinetics of the films have been analyzed using Tafel slopes, which are shown in Fig. 7b. The Tafel slopes are measured to be 196, 217, 230 mV/decade for the NiO films grown on $SrTiO_3$, $LaAlO_3$, and Al_2O_3, respectively. These results demonstrate the dependence of the NiO's catalytic behavior on the substrate. The Nyquist plots obtained at 0.6 V vs. Hg/HgO are shown in Fig. 7c. The radii of semicircular Nyquist plots represent the charge transfer resistance; the smaller is the radius, the smaller is the charge transfer resistance and hence the faster is the reaction kinetics [14]. Thus, as seen in the Nyquist plots in Fig. 7c, NiO film on STO has the smallest radius among all the films, indicating the least charge transfer resistance, and hence, the best electrochemical catalytic behavior. The NiO films on $LaAlO_3$ and Al_2O_3 follow the suit. Fig. 7d shows the relation between the lattice strain and overpotential of NiO thin films. The bottom x-axis represents the substrate-induced external strain (ε_{ext}) and top x-axis represents the internal strain (ε_{int}

Table 1
Parameters extracted from NiO thin films.

Substrate	FWHM	Grain size(nm)	Surface roughness(nm)	%Lattice strain (ε)	Dislocation Density (10^{15} m^2)
$SrTiO_3$	0.254	34	9.7	7	0.9
$LaAlO_3$	0.284	30	3.6	10	1.1
Al_2O_3	0.450	22	1.6	12	1.9

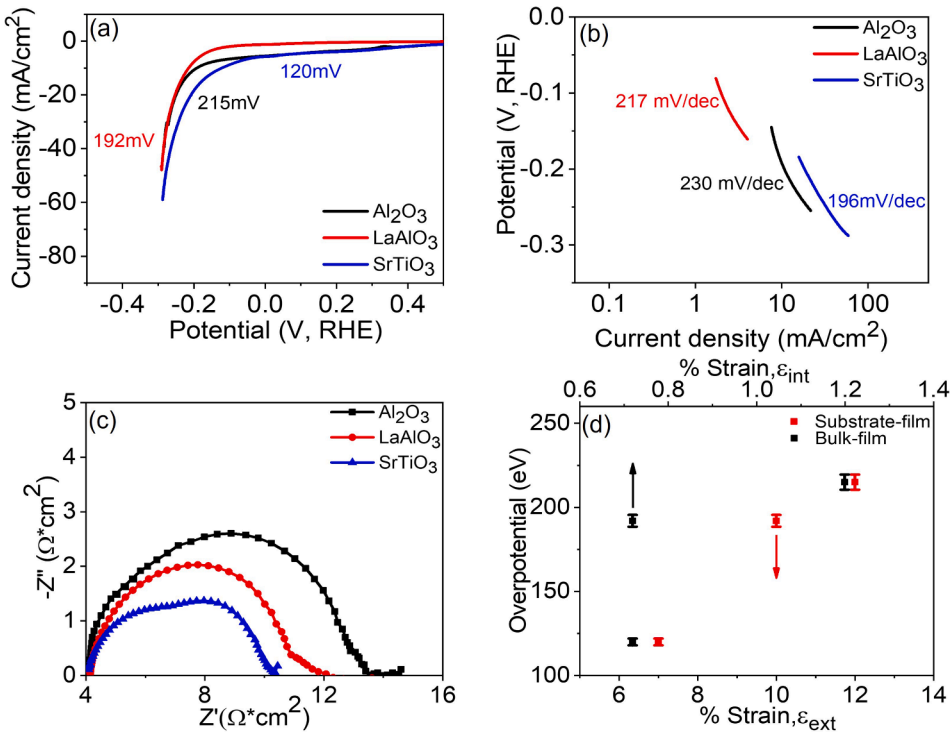

Fig. 7. (a) Polarization curves, (b) Tafel Slopes, and (c) Nyquist plots for the NiO thin film grown on Al_2O_3, $LaAlO_3$, and $SrTiO_3$ substrates (d) Variation of overpotential with lattice strain for as-deposited NiO thin films.

= $[a_b - a_f]/a_f$, where a_b and a_f are the bulk and film lattice parameters, respectively) in the NiO films. The internal NiO strain is almost an order of magnitude smaller than the substrate-induced external NiO lattice strain. However, the trend of the effect of both strains on the HER overpotential is similar; the overpotential increases as the strain in the NiO film increases.

The cyclic voltammograms (CVs) of the three samples are shown in Fig. 8a. All three voltammograms displayed oxidation/reduction peaks. The specific capacitance, obtained by dividing the area under the CV curves by the product of the potential range and scan rate, is plotted as a function of current density in Fig. 8b. It can be observed from this figure that the NiO/$SrTiO_3$ and NiO/Al_2O_3 electrodes displayed, respectively, the highest and lowest values of specific capacitance, in all current density range used in the present study with NiO/Al_2O_3 electrodes showing in between behavior. The specific capacitance values for NiO on the three substrates are plotted as function of their overpotential in the inset of Fig. 8b. The monotonic decrease of specific capacitance with an increase in overpotential can be taken as an evidence of electron conduction between electrolyte and the NiO electrodes. The enhanced storage behavior of the NiO thin film on the $SrTiO_3$ substrate (even at higher current densities) may be attributed to the lower resistivity at the NiO/$SrTiO_3$ interface due to the smaller lattice strain and the increased active sites for storage due to the enhanced surface roughness. Conversely, the NiO/Al_2O_3 interface had the highest lattice strain density and, therefore, electrical resistivity. This situation hampers access to the active sites for electrochemistry. The NiO films were also tested for their electrochemical stability; the results obtained is presented in Fig. 8c. The stability test was carried out at an applied voltage of 1.65 V vs. RHE. The results show that the decay of current density of the NiO/$SrTiO_3$ and NiO/$LaAlO_3$ samples were almost negligible while NiO/Al2O3 samples showed a slight degradation in the 45-hour timespan of testing.

4. Conclusions

NiO thin films have been fabricated on three different substrates using PLD. The effect of the lattice strain in the NiO thin films, brought about by the substrate-film lattice mismatch, on the HER overpotential and pseudocapacitive Ni redox have been investigated. Linear sweep voltammetry data shows that the overpotential value of NiO thin films on the $SrTiO_3$ substrate is up to 1.8 times lower at a lattice strain of 7% compared to Al_2O_3 substrate with the highest lattice strain of 12%. It is also evident from the Nyquist plot that the $SrTiO_3$/NiO sample has the fastest reaction kinetic rate among the other samples in this study. The specific capacitance was recorded for all samples, and the NiO/$SrTiO_3$ sample recorded the highest value of 172 mF/cm^2. The substrate material is an important factor in the electrochemical system since the substrate-film lattice mismatch influences the strain and the storage capabilities of the electrode. The results could be technologically more practical if NiO films were grown on conducting substrates. However, for better control of structural orientation, grain size, and epitaxy, the present study was carried out on three well-known single crystal substrates.

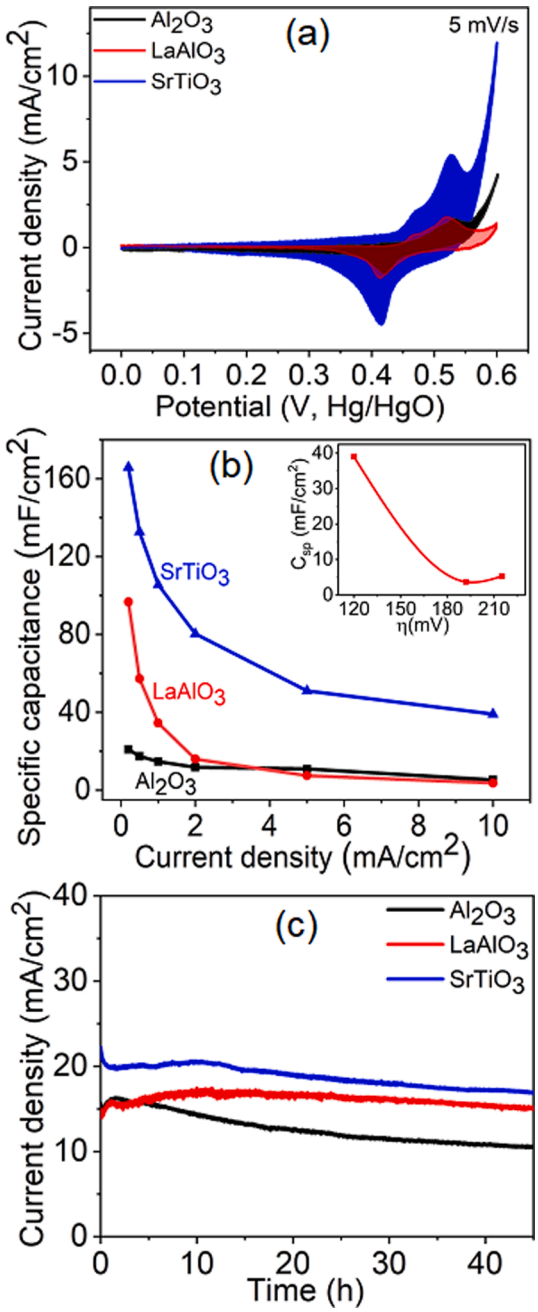

Fig. 8. (a) Cyclic voltammogram as a function of potential at 5 mV/s scan rate (b) specific capacitance as a function of current density (c) time-dependent current density plots for the NiO films.

Funding

The authors would like to acknowledge the financial support from the NSF PREM grant [Grant Numbers DMR-2122067] and NSF Major Research Instrumentation (MRI) program [Grant Number CMMI-1040290].

Data availability statement

The raw/processed data required to reproduce these findings cannot be shared at this time due to technical or time limitations.

Declaration of Competing Interest

The authors declare that they have no known competing financial interests or personal relationships that could have appeared to influence the work reported in this paper.

References

[1] F.M. Sapountzi, J.M. Gracia, C.J. Weststrate, H.O.A. Fredriksson, J. W. Niemantsverdriet, Electrocatalysts for the generation of hydrogen, oxygen and synthesis gas, Prog. Energy Combust. Sci. 58 (2017) 1–35, https://doi.org/10.1016/j.pecs.2016.09.001.

[2] D.L. Capuano, U.S. Energy Information Administration's International Energy Outlook 2020(IEO2020). Accessed on: Feb. 3, 2021. [Online]. Available: https://www.eia.gov/outlooks/ieo/.

[3] F.P. Perera, Multiple Threats to Child Health from Fossil Fuel Combustion: Impacts of Air Pollution and Climate Change, Environ. Health Perspect. 125 (2) (2017) 141–148, https://doi.org/10.1289/EHP299.

[4] B.K. Bose, Global Warming: Energy, Environmental Pollution, and the Impact of Power Electronics, IEEE Ind. Electron. Mag. 4 (1) (2010) 6–17, https://doi.org/10.1109/MIE.2010.935860.

[5] P.C. Jain, Greenhouse effect and climate change: scientific basis and overview, Renewable Energy 3 (4) (1993) 403–420, https://doi.org/10.1016/0960-1481(93)90108-S.

[6] P.T. Babar, A.C. Lokhande, M.G. Gang, B.S. Pawar, S.M. Pawar, J.H. Kim, Thermally oxidized porous NiO as an efficient oxygen evolution reaction (OER) electrocatalyst for electrochemical water splitting application, J. Ind. Eng. Chem. 60 (2018) 493–497, https://doi.org/10.1016/j.jiec.2017.11.037.

[7] A. Saeedmanesh, M.A. Mac Kinnon, J. Brouwer, Hydrogen is essential for sustainability, Curr. Opin. Electrochem. 12 (2018) 166–181, https://doi.org/10.1016/j.coelec.2018.11.009.

[8] Z. Ge, B. Fu, J. Zhao, X. Li, B. Ma, Y. Chen, A review of the electrocatalysts on hydrogen evolution reaction with an emphasis on Fe, Co and Ni-based phosphides, J. Mater. Sci. 55 (29) (2020) 14081–14104, https://doi.org/10.1007/s10853-020-05010-w.

[9] S.A. Sherif, F. Barbir, T.N. Veziroglu, Principles of hydrogen energy production, storage and utilization, 2003.

[10] X. Yan, L. Tian, X. Chen, Crystalline/amorphous Ni/NiO core/shell nanosheets as highly active electrocatalysts for hydrogen evolution reaction, J. Power Sources 300 (2015) 336–343.

[11] P. Breeze, in: Power System Energy Storage Technologies, Elsevier, 2018, pp. 69–77, https://doi.org/10.1016/B978-0-12-812902-9.00008-0.

[12] C. Lv, Z. Peng, Y. Zhao, Z. Huang, C. Zhang, The hierarchical nanowires array of iron phosphide integrated on a carbon fiber paper as an effective electrocatalyst for hydrogen generation, J. Mater. Chem. A 4 (4) (2016) 1454–1460.

[13] B. Mu, A. Wang, Fabrication and Applications of Carbon/Clay Mineral Nanocomposites, in: Nanomaterials from Clay Minerals: Elsevier, 2019, pp. 537–587.

[14] N.R. Mucha, J. Som, J. Choi, S. Shaji, R.K. Gupta, H.M. Meyer, C.L. Cramer, A. M. Elliot, D. Kumar, High-Performance Titanium Oxynitride Thin Films for Electrocatalytic Water Oxidation, ACS Appl. Energy Mater. 3 (9) (2020) 8366–8374, https://doi.org/10.1021/acsaem.0c00988.

[15] W. Zhang, W. Lai, R. Cao, Energy-Related Small Molecule Activation Reactions: Oxygen Reduction and Hydrogen and Oxygen Evolution Reactions Catalyzed by Porphyrin- and Corrole-Based Systems, Chem. Rev. 117 (4) (2017) 3717–3797, https://doi.org/10.1021/acs.chemrev.6b00299.

[16] Q. Zhao, Z. Yan, C. Chen, J. Chen, Spinels: Controlled Preparation, Oxygen Reduction/Evolution Reaction Application, and Beyond, Chem. Rev. 117 (15) (2017) 10121–10211, https://doi.org/10.1021/acs.chemrev.7b00051.

[17] V. Vij, S. Sultan, A.M. Harzandi, A. Meena, J.N. Tiwari, W.-G. Lee, T. Yoon, K. S. Kim, Nickel-based electrocatalysts for energy-related applications: oxygen reduction, oxygen evolution, and hydrogen evolution reactions, ACS Catal. 7 (10) (2017) 7196–7225.

[18] G.-J. Hwang, B.-M. Gil, C.-H. Ryu, Preparation of the electrode using NiFe2O4 powder for the alkaline water electrolysis, J. Ind. Eng. Chem. 48 (2017) 242–248, https://doi.org/10.1016/j.jiec.2017.01.011.

[19] T. Tian, L. Huang, L. Ai, J. Jiang, Surface anion-rich NiS 2 hollow microspheres derived from metal–organic frameworks as a robust electrocatalyst for the hydrogen evolution reaction, J. Mater. Chem. A 5 (39) (2017) 20985–20992.

[20] M. Bonomo, D. Dini, F. Decker, Electrochemical and Photoelectrochemical Properties of Nickel Oxide (NiO) With Nanostructured Morphology for Photoconversion Applications (in English), Front. Chem. 6 (2018), https://doi.org/10.3389/fchem.2018.00601.

[21] J. Liang, Y.-Z. Wang, C.-C. Wang, S.-Y. Lu, In situ formation of NiO on Ni foam prepared with a novel leaven dough method as an outstanding electrocatalyst for oxygen evolution reactions, J. Mater. Chem. A 4 (25) (2016) 9797–9806.

[22] J. Guo, W. Fu, H. Yang, Q. Yu, W. Zhao, X. Zhou, Y. Sui, J. Ding, Y. Li, S. Cheng, M. Li, A NiO/TiO2junction electrode constructed using self-organized TiO2nanotube arrays for highly efficient photoelectrocatalytic visible light activations, J. Phys. D Appl. Phys. 43 (24) (2010) 245202, https://doi.org/10.1088/0022-3727/43/24/245202.

[23] N.R. Mucha, J. Som, S. Shaji, S. Fialkova, P.R. Apte, B. Balasubramanian, J. E. Shield, M. Anderson, D. Kumar, Electrical and optical properties of titanium

oxynitride thin films, J. Mater. Sci. 55 (12) (2020) 5123–5134, https://doi.org/10.1007/s10853-019-04278-x.

[24] A.N. Buckley, R. Woods, Electrochemical and XPS studies of the surface oxidation of synthetic heazlewoodite (Ni3S2), J. Appl. Electrochem. 21 (7) (1991) 575–582, https://doi.org/10.1007/BF01024844.

[25] P.W. Menezes, A. Indra, C. Das, C. Walter, C. Göbel, V. Gutkin, D. Schmeiβer, M. Driess, Uncovering the Nature of Active Species of Nickel Phosphide Catalysts in High-Performance Electrochemical Overall Water Splitting, ACS Catal. 7 (1) (2017) 103–109, https://doi.org/10.1021/acscatal.6b02666.

[26] K. Fominykh, J.M. Feckl, J. Sicklinger, M. Döblinger, S. Böcklein, J. Ziegler, J. Ziegler, L. Peter, J. Rathousky, E.-W. Scheidt, T. Bein, D.-F. Rohlfing, Ultrasmall Dispersible Crystalline Nickel Oxide Nanoparticles as High-Performance Catalysts for Electrochemical Water Splitting, Adv. Funct. Mater. 24 (21) (2014) 3123–3129, https://doi.org/10.1002/adfm.201303600.

[27] K. Sun, F.H. Saadi, M.F. Lichterman, W.G. Hale, H.-P. Wang, X. Zhou, N.T. Plymale, S.T. Omelchenko, J.-H. He, K.M. Papadantonakis, B.S. Brunschwig, N.S. Lewis, "Stable solar-driven oxidation of water by semiconducting photoanodes protected by transparent catalytic nickel oxide films," (in eng), Proc. Natl. Acad. Sci. U S A 112 (12) (2015) 3612–3617, https://doi.org/10.1073/pnas.1423034112.

[28] V.P. Patil, S. Pawar, M. Chougule, P. Godse, R. Sakhare, S. Sen, P. Joshi, Effect of Annealing on Structural, Morphological, Electrical and Optical Studies of Nickel Oxide Thin Films, JSEMAT 01 (02) (2011) 35–41.

[29] I. Porqueras, E. Bertran, Electrochromic behaviour of nickel oxide thin films deposited by thermal evaporation, Thin Solid Films 398–399 (2001) 41–44, https://doi.org/10.1016/S0040-6090(01)01301-3.

[30] B. Subramanian, M. Mohamed Ibrahim, V. Senthilkumar, K.R. Murali, V.S. Vidhya, C. Sanjeeviraja, M. Jayachandran, Optoelectronic and electrochemical properties of nickel oxide (NiO) films deposited by DC reactive magnetron sputtering, Physica B 403 (21-22) (2008) 4104–4110.

[31] P.S. Patil, L.D. Kadam, Preparation and characterization of spray pyrolyzed nickel oxide (NiO) thin films, Appl. Surf. Sci. 199 (1) (2002) 211–221, https://doi.org/10.1016/S0169-4332(02)00839-5.

[32] L. Ai, G. Fang, L. Yuan, N. Liu, M. Wang, C. Li, Q. Zhang, J. Li, X. Zhao, Influence of substrate temperature on electrical and optical properties of p-type semitransparent conductive nickel oxide thin films deposited by radio frequency sputtering, Appl. Surf. Sci. 254 (8) (2008) 2401–2405, https://doi.org/10.1016/j.apsusc.2007.09.051.

[33] M. Tanaka, M. Mukai, Y. Fujimori, M. Kondoh, Y. Tasaka, H. Baba, S. Usami, Transition metal oxide films prepared by pulsed laser deposition for atomic beam detection, Thin Solid Films 281–282 (1996) 453–456, https://doi.org/10.1016/0040-6090(96)08673-7.

[34] M. Roy, N.R. Mucha, S. Fialkova, D. Kumar, Effect of thickness on metal-to-semiconductor transition in 2-dimensional TiN thin films, AIP Adv. 11 (4) (2021) 045204, https://doi.org/10.1063/5.0046243.

[35] N.R. Mucha, M. Roy, C.S.R. Nannuri, D. Kumar, H. Rathnayake, Bandgap engineering of oxinitride nanowires for water splitting and hydrogen generation, in: APS March Meeting Abstracts, 2018, vol. 2018, p. G60. 311.

[36] K. Sarkar, P. Jaipan, J. Choi, T. Haywood, D. Tran, N.R. Mucha, S. Yarmolenko, O. Scott-Emuakpor, M. Sundaresan, R.K. Gupta, D. Kumar, Enhancement in corrosion resistance and vibration damping performance in titanium by titanium nitride coating, SN Appl. Sci. 2 (5) (2020) 1–14.

[37] S. Jin, Y. Zhu, Z. He, H. Chen, X.i. Liu, F. Li, J. Liu, M. Liu, Y. Chen, Revealing the effects of oxygen defects on the electro-catalytic activity of nickel oxide, Int. J. Hydrogen Energy 45 (1) (2020) 424–432.

[38] A.C. Sonavane, A.I. Inamdar, P.S. Shinde, H.P. Deshmukh, R.S. Patil, P.S. Patil, Efficient electrochromic nickel oxide thin films by electrodeposition, J. Alloy. Compd. 489 (2) (2010) 667–673, https://doi.org/10.1016/j.jallcom.2009.09.146.

[39] M.-S. Wu, Y.-A. Huang, C.-H. Yang, J.-J. Jow, Electrodeposition of nanoporous nickel oxide film for electrochemical capacitors, Int. J. Hydrogen Energy 32 (17) (2007) 4153–4159, https://doi.org/10.1016/j.ijhydene.2007.06.001.

[40] A.-R. Khadher, M. Farooqui, G. Rabbani, Nickel Oxide Thin Film Synthesis by Sol-Gel Method on Glass Substrates.

[41] L.-F. Huang, M. Hutchison, R. Santucci Jr, J.R. Scully, J.M. Rondinelli, Improved electrochemical phase diagrams from theory and experiment: the Ni–water system and its complex compounds, J. Phys. Chem. C 121 (18) (2017) 9782–9789.

[42] Y. Zhu, H. Guo, Y.u. Wu, C. Cao, S. Tao, Z. Wu, Surface-enabled superior lithium storage of high-quality ultrathin NiO nanosheets, J. Mater. Chem. A 2 (21) (2014) 7904, https://doi.org/10.1039/c4ta00257a.

[43] Z. Tan, W. Zhang, D. Qian, C. Cui, Q.i. Xu, L. Li, S. Li, Y. Li, Solution-processed nickel acetate as hole collection layer for polymer solar cells, Phys. Chem. Chem. Phys. 14 (41) (2012) 14217, https://doi.org/10.1039/c2cp41465a.

[44] J. Liu, W. Lv, W. Wei, C. Zhang, Z. Li, B. Li, F. Kang, Q.-H. Yang, A three-dimensional graphene skeleton as a fast electron and ion transport network for electrochemical applications, J. Mater. Chem. A 2 (9) (2014) 3031, https://doi.org/10.1039/c3ta14315e.

[45] U. Holzwarth, N. Gibson, The Scherrer equation versus the 'Debye-Scherrer equation', Nat. Nanotechnol. 6 (9) (2011) 534, https://doi.org/10.1038/nnano.2011.145.

[46] W. Ramadan, S. Ogale, S. Dhar, S. Zhang, D. Kundaliya, T. Venkatesan, Substrate-induced strain effects on the transport properties of pulsed laser-deposited Nb-doped Sr Ti O 3 films, Appl. Phys. Lett. 88 (14) (2006), 142903.

[47] P. Salunkhe, M. A. AV, D. Kekuda, Investigation on tailoring physical properties of Nickel Oxide thin films grown by dc magnetron sputtering, Mater. Res. Exp. 7 (1) (2020) 016427.

[48] L.C. Seitz, C.F. Dikens, K. Nishio, Y. Hikita, J. Montoya, A. Doyle, C. Kirk, A. Vojvodic, H.Y. Hwang, J.K. Norskov, T.F. Jaramillo, A highly active and stable $IrO_x/SrIrO_x$ catalyst for the oxygen evolution reaction, Science 353 (6303) (2016) 1011, https://doi.org/10.1126/science.aaf5050.

[49] K.A. Stoerzinger, M. Risch, J. Suntivich, W.M. Lü, J. Zhou, M.D. Biegalski, H. M. Christen, Ariando, T. Venkatesan, Y. Shao-Horn, Oxygen electrocatalysis on (001)-oriented manganese perovskite films: Mn valency and charge transfer at the nanoscale, Energy Environ. Sci. 6 (5) (2013) 1582, https://doi.org/10.1039/c3ee40321a.